ARL-TR-7401 ● AUG 2015

US Army Research Laboratory

Conductivity of Hot Isostatically Pressed $Li_{0.35}La_{0.55}TiO_3$

by Jeff Wolfenstine, Jan Allen, Claire Weiss Brennan, and Victoria Blair

NOTICES

Disclaimers

The findings in this report are not to be construed as an official Department of the Army position unless so designated by other authorized documents.

Citation of manufacturer's or trade names does not constitute an official endorsement or approval of the use thereof.

Destroy this report when it is no longer needed. Do not return it to the originator.

ARL-TR-7401 ● AUG 2015

US Army Research Laboratory

Conductivity of Hot Isostatically Pressed $Li_{0.35}La_{0.55}TiO_3$

by Jeff Wolfenstine and Jan Allen
Sensors and Electron Devices Directorate, ARL

Claire Weiss Brennan and Victoria Blair
Weapons and Material Research Directorate, ARL

REPORT DOCUMENTATION PAGE

Form Approved
OMB No. 0704-0188

1. REPORT DATE *(DD-MM-YYYY)*	2. REPORT TYPE	3. DATES COVERED (From - To)
Aug 2015	Final	06/2015

4. TITLE AND SUBTITLE
Conductivity of Hot Isostatically Pressed $Li_{0.35}La_{0.55}TiO_3$

5a. CONTRACT NUMBER

5b. GRANT NUMBER

5c. PROGRAM ELEMENT NUMBER

6. AUTHOR(S)
Jeff Wolfenstine, Jan Allen, Claire Weiss Brennan, and Victoria Blair

5d. PROJECT NUMBER

5e. TASK NUMBER

5f. WORK UNIT NUMBER

7. PERFORMING ORGANIZATION NAME(S) AND ADDRESS(ES)
US Army Research Laboratory
ATTN: RDRL-SED-C
2800 Powder Mill Road
Adelphi, MD 20783-1138

8. PERFORMING ORGANIZATION REPORT NUMBER
ARL-TR-7401

9. SPONSORING/MONITORING AGENCY NAME(S) AND ADDRESS(ES)

10. SPONSOR/MONITOR'S ACRONYM(S)

11. SPONSOR/MONITOR'S REPORT NUMBER(S)

12. DISTRIBUTION/AVAILABILITY STATEMENT
Approved for public release; distribution is unlimited.

13. SUPPLEMENTARY NOTES

14. ABSTRACT
The ionic conductivity of $Li_{0.35}La_{0.55}TiO_3$ (LLTO) consolidated using a 2-stage method of solid-state sintering followed by hot isostatic pressing (hipping) was measured and compared to LLTO densified using conventional solid-state sintering. After sintering and hipping, the LLTO material exhibited near full theoretical density (relative density~99%), a cubic structure, grain size~2.42 μm), and clean grain boundaries with no secondary phases. The room temperature grain boundary conductivity values were ~3.8×10^{-5} S/cm for the sintered and hipped LLTO. Although the sintered and hipped LLTO had a density near full theoretical density, the total conductivity is still somewhat low compared to the value for lattice conductivity (~1.5×10^{-3} S/cm). These results suggest that in order to increase the grain boundary conductivity of LLTO, achieving full theoretical density alone is not sufficient; the addition of a Li-ion conducting phase along grain boundaries is required.

15. SUBJECT TERMS
hipping, grain boundary, ionic conductivity, cubic, pervoskite

16. SECURITY CLASSIFICATION OF:			17. LIMITATION OF ABSTRACT	18. NUMBER OF PAGES	19a. NAME OF RESPONSIBLE PERSON
a. REPORT	b. ABSTRACT	c. THIS PAGE			Jeff Wolfenstine
Unclassified	Unclassified	Unclassified	UU	24	19b. TELEPHONE NUMBER (Include area code) 301-394-0317

Contents

List of Figures

Acknowledgments

We gratefully acknowledge support of the US Army Research Laboratory.

INTENTIONALLY LEFT BLANK.

1. Introduction

Recently, there has been interest in the development of lithium (Li)-Air batteries for use in high energy applications at room temperature. One configuration involves the use of a Li anode in a non-aqueous electrolyte, an open-air cathode in an aqueous electrolyte, and a Li-ion conducting membrane that separates the 2 electrolytes.[1,2] This membrane must possess high relative density, high Li-ion conductivity, low electronic conductivity, high mechanical strength, and excellent chemical stability.[1,2] Ceramic electrolytes offer several of these needed characteristics. $Li_{3x}La_{(2/3)-x}TiO_3$ (LLTO) is a promising candidate for use as a membrane. One reason LLTO is under consideration is that among Li-ion conducting ceramics, it has one of the highest reported room temperature Li-ion lattice conductivity values, ~$1x10^{-3}$ S/cm.[3–5] For it to be used in practical applications, however, a dense polycrystalline material is required. In most cases, conventional solid-state sintering is used to consolidate the LLTO powders into a dense polycrystalline material.[5] The total ionic conductivity of a polycrystalline material is a function of both the lattice and grain boundary contributions.[6–8] In general, Li-ion conduction through the grain boundaries limits the total conductivity of LLTO at room temperature to typically less than 10^{-5} S/cm.[5,9–13] A possible reason for this low value of total conductivity compared to the lattice conductivity is a result of porosity along grain boundaries.[9–12] It was suggested that if this porosity could be removed, the total conductivity of LLTO would approach values for lattice conductivity.[9] One possible way to remove this porosity—hence, increasing both room temperature grain boundary conductivity and total conductivity—is to follow conventional solid-state sintering, to a obtain a porosity level of about <5%, with hot isostatic pressing (hipping) to eliminate the remaining 5% porosity to achieve full theoretical density. This procedure will not cause degradation in the mechanical properties. In fact, it has been shown that this procedure lead to LLTO with less than 1% porosity (relative density ~99%), with increased fracture strength and elastic modulus values compared to LLTO consolidated by solid-state sintering.[14] Additionally, this sintering and hipping approach has the potential for consolidating complex shapes (for example, ceramic tubes with one closed end) to near theoretical density, which may be required in certain applications. Hence, the purpose of this short note is to determine if the combined method of solid-state sintering followed by hipping will lead to LLTO with near full theoretical density (relative density ~99%); additionally, perhaps this will, in turn, lead to high with room temperature grain boundary conductivity and, hence, a total conductivity approaching values for lattice conductivity.

2. Experimental

2.1 Powder Preparation

The $Li_{0.35}La_{0.55}iO_3$ stoichiometry was chosen for this study because this composition is known to crystallize a higher proportion of cubic phase than other compositions. However, to get pure cubic phase, the material must be quenched from >1150 °C.[5,13,15] The cubic phase can have a lattice conductivity up to 2–3 times higher than the tetragonal phase.[5,13,15] The starting powder was formed from a mixture of Li_2CO_3, $La_2(CO_3)_3$•$8H_2O$, and TiO_2, as described previously.[9,14] A 10 wt% excess of Li_2CO_3 was used to account for possible volatilization of Li-containing species during high temperature synthesis. The starting materials were mixed in an aqueous slurry for 1 h, after which the water was removed by rotary evaporation. The powder cake was coarsely broken and transferred to a clean, loosely covered container, where it was left to stand for 1–2 days to allow for complete solvent volatilization. After drying, the powder was sieved through a 58 mesh nylon screen and then jet milled (The Jet Pulverizer Company Inc.) to homogenize the powder particle size and composition. The powder was then calcined in alumina crucibles by heating in an open air furnace at 1150 °C for 1 h (both heating and cooling ramp rates were 2.5 °C/min). After heating, the powder is slightly coarsened and so was subjected to a second cycle of sieving and jet milling before sintering.

2.2 Consolidation

Six LLTO samples were prepared for sintering and hipping by first compacting the powder in a uniaxial press to 16.8 MPa in a 31.75 mm diameter stainless steel die. The cold-pressed discs were vacuum-sealed in a plastic bag for cold-isostatic pressing to 207 MPa. After cold-isostatic pressing, the samples were then sintered under air. The sintering and hipping temperature of 1200 °C was selected because thermal analysis suggested that $Li_{0.35}La_{0.55}TiO_3$ melts at temperatures above 1250 °C.[16,17] For solid-state sintering, the furnace temperature was ramped to 800 ºC at 5 ºC/min then slowed to 2º/min to 1200 ºC, isothermally held for 6 h, and cooled to room temperature at 3 ºC/min. Hipping of the 6 sintered samples was performed in a high pressure furnace at American Isostatic Presses, Inc., (Columbus, OH, USA). For both the sintering and hipping samples were covered with loose LLTO powder to prevent Li loss. The samples were heated at 1200 ºC for 5 h under an atmosphere of 20% oxygen: 80% argon at 310 MPa. Heating and cooling rates were 10 ºC/min.

2.3 Physical Characterization

The bulk density of all 6 sintered and hipped LLTO materials was measured via the Archimedes method, using water as the immersion fluid. Powder X-ray diffraction (XRD) analysis was employed to determine the crystalline phases present in all 6 LLTO samples after sintering and hipping. A Scanning Electron Microscope (SEM) was used to observe the microstructure of hipped LLTO on polished and etched or fractured surfaces. SEM samples were prepared by polishing with a diamond slurry of progressively smaller average particle size down to 0.25 μm. The polished samples were thermally etched at 1100 ºC for 1 h (5º/min heating and cooling rate) under air. No surface coatings were applied to examine the polished and etched or fractured samples, but low accelerating voltages of 2 or 5 kV were used to minimize surface charging during SEM operation. The grain size was determined using the intercept method from the micrographs using the relation, D=1.56 C/MN, where C is the length of an arbitrarily placed line on the micrograph, M is the magnification, and N is the number of grain boundary intercepts across the line.[18] Transmission electron microscopy (TEM) and scanning transmission electron microscopy (STEM) imaging was done using the JEOL JEM-2100F. The TEM samples were prepared by cutting the LLTO using a diamond saw, thinning to approximately 50 μm via mechanical polishing using progressively finer diamond films down to 3 μm, and final thinning was done using the focused ion beam (FIB) milling instrument. For FIB milling, the ~50 μm polished LLTO sample was mounted on a tabbed 1 mm × 2 mm oval-hole TEM half-grid using Epo-Tek® 353-ND epoxy. The grid-mounted sample was then thinned to electron transparency using the FEI Nova600 dual beam FIB in the traditional "H-bar orientation," where multiple thin sections for TEM analysis can be prepared on 1 TEM grid.

2.4 Electrical Characterization

LLTO rectangular parallelepipeds samples of approximately 12 mm × 12 mm × 1 mm thick were cut using a low-speed diamond saw from all 6 sintered and hipped discs for electrical characterization. The top and bottom faces were polished with SiC paper using mineral oil as a lubricant. All polishing was done in a glove box with an oxygen and water content less than 1 ppm. The purpose of polishing in a glove box was to insure removal of any surface films (i.e., Li_2CO_3) that may have formed during exposure of the LLTO sample to ambient air at room temperature during handling after the sintering and hipping steps prior to electrical characterization.[19] All samples were stored in the glove box when not in use. Pt was sputter-coated on to the top and bottom surfaces of the specimens. Electrical conductivity measurements were performed on the Pt coated samples using the

2-probe method. Room temperature Li-ion conductivity was determined from AC electrochemical impedance spectroscopy (EIS) using a Bio-logic SP200 over a frequency range of 0.1 Hz–7 MHz with a potential amplitude of 100 mV. The bulk, grain boundary, and electrode contributions to the impedance spectra were separated by fitting the spectra using ZView (Scribner Associates, Inc.). The DC polarization steady-state current and 2 V potential were used to determine the resistance, which was converted to electronic conductivity using the specimen dimensions.

3. Results and Discussion

A typical XRD pattern of a sintered and hipped LLTO sample is shown in Fig. 1. From Fig. 1, the major peaks in the diffraction pattern can be indexed to the cubic structure of LLTO (PDF# 46-465). The % of tetragonal phase (shown by stars in Fig. 1) determined using Rietveld refinement was about 3 wt.% or less for all samples. Representative SEM micrographs of the sintered and hipped LLTO are shown in Figs. 2 and 3. Figure 2 is an SEM image of a polished and thermally etched surface; Fig. 3 is an SEM image of a fracture surface. From Figs. 2 and 3, several important points are noted. First, very little porosity is observed, in agreement with the relative density of ~99% (99 ± 1% for the six samples) determined using the Archimedes method. A majority of the porosity is located along grain boundaries or at triple junctions. Second, no individual grains larger than 5 μm can be observed. Third, irregular grain growth is not evident. Fourth, the grain size of the sintered and hipped LLTO samples varied between 2.01–2.72 μm, yielding an average grain size of 2.42 ± 0.15 μm. Fifth, the fracture mode is a mixture of transgranular and intergranular fracture.

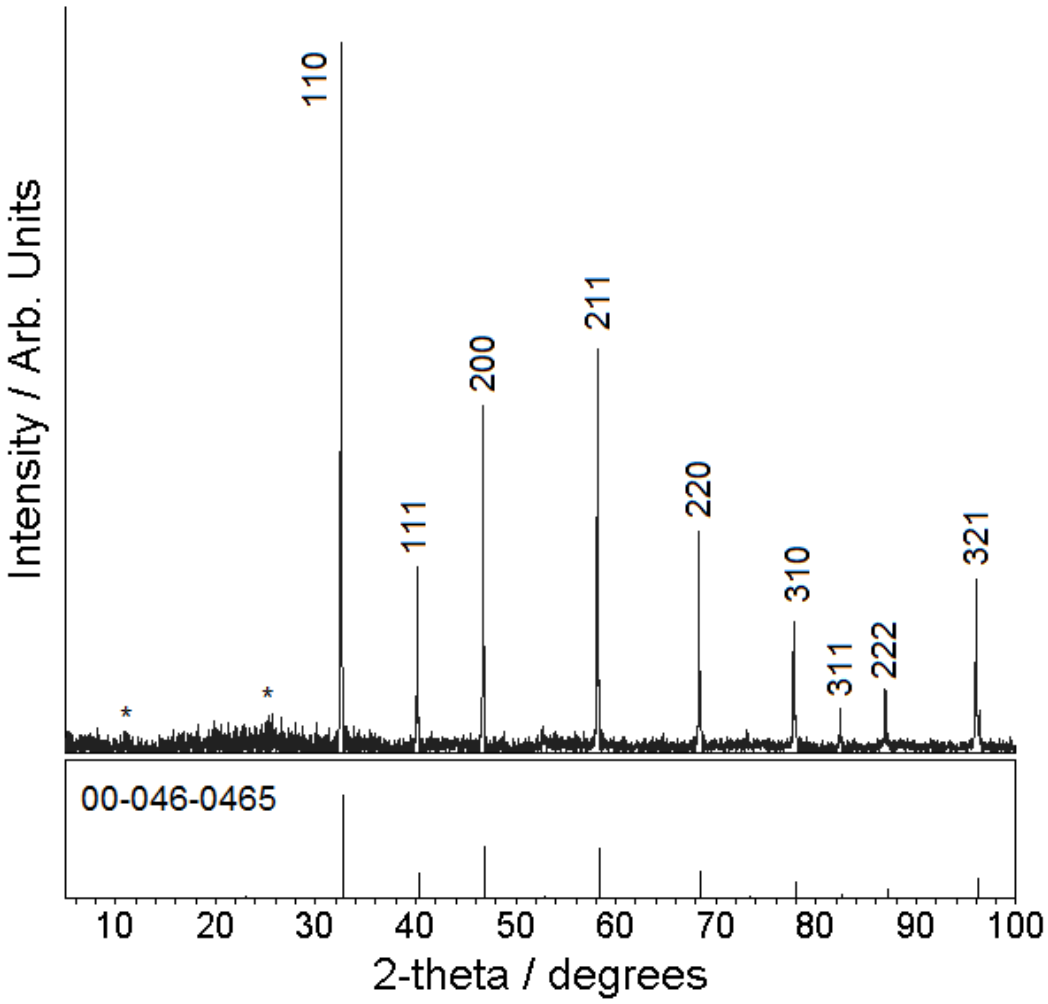

Fig. 1 X-ray diffraction pattern of sintered and hipped $Li_{0.35}La_{0.55}TiO_3$

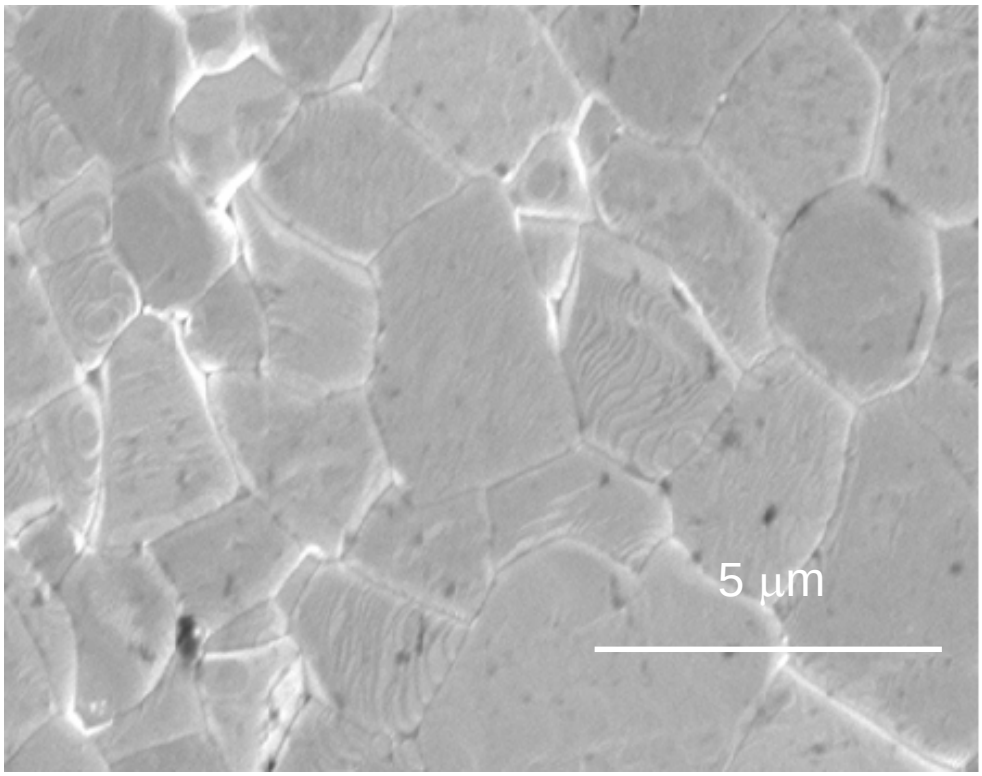

Fig. 2 Scanning electron micrograph of polished and thermal etched $Li_{0.35}La_{0.55}TiO_3$

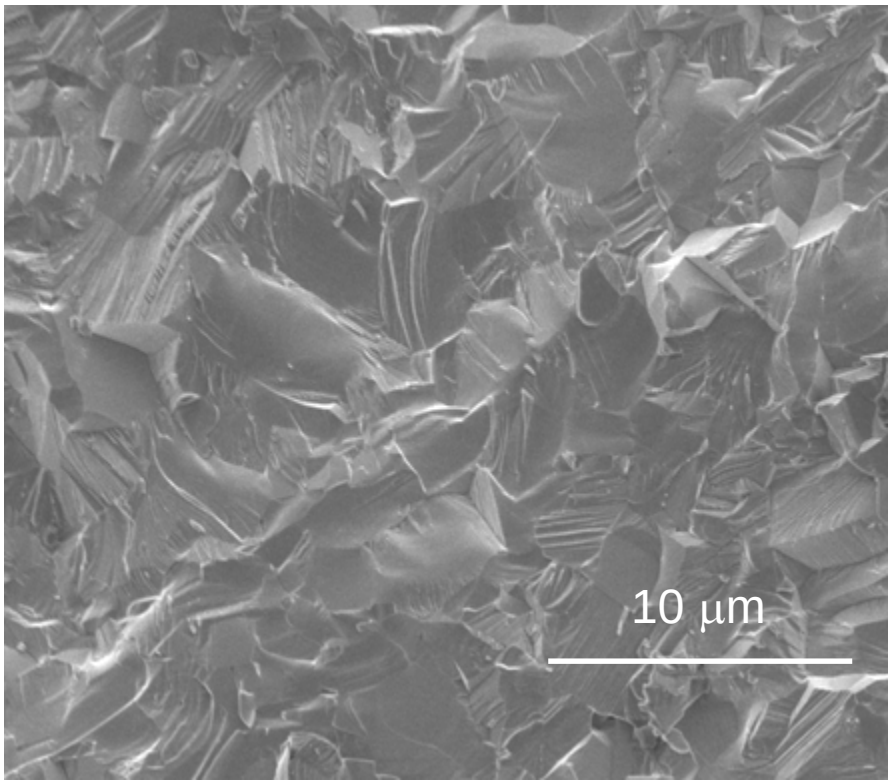

Fig. 3 Scanning electron micrograph of a $Li_{0.35}La_{0.55}TiO_3$ fracture surface

High-angle annular dark field (HAADF) STEM and bright-field TEM imaging were used to study the Z-contrast and the grain boundaries, respectively. In HAADF STEM, the image contrast is sensitive to the average atomic number, and in Fig. 4, the dark regions represent areas of lower average atomic number as compared to the bulk LLTO. These darker regions (indicated by arrows in Figs. 4a and 4b) were determined to be microvoids, since they appear as dark contrast in HAADF STEM and as extremely bright contrast in bright field TEM (not shown). The very high brightness contrast in bright field TEM indicates enhanced electron transmission through that portion of the sample. The microvoids observed in LLTO appear almost exclusively along grain boundaries and at triple junctions of certain LLTO grains, not within the grain interior. High-resolution bright field TEM images (Figs. 4c and 4d) were used to examine the nature of the grain boundaries in the sintered and hipped LLTO ceramics. In Fig. 4c, we note that the grain boundary is clean, with no secondary phases observed. In order to study the grain boundaries in more detail, the sample was tilted relative to the electron beam such that both of the neighboring grains lie in low index zone axis orientations. The crystallographic orientations of the grains located on either side of the grain boundary of interest are determined using convergent beam electron diffraction (CBED). Then, the sample is tilted until the CBED patterns indicate that both grains lie in low index zones. This process to image the grain boundaries helps to minimize the apparent thickness of the grain boundary and is extremely useful for studying secondary phases and/or amorphous regions at grain boundaries. This tilting process was used for Fig. 4d, in which the LLTO lattice can be seen on either side of the grain boundary, and the grain boundary, itself, has a very narrow width, with no amorphous regions observed.

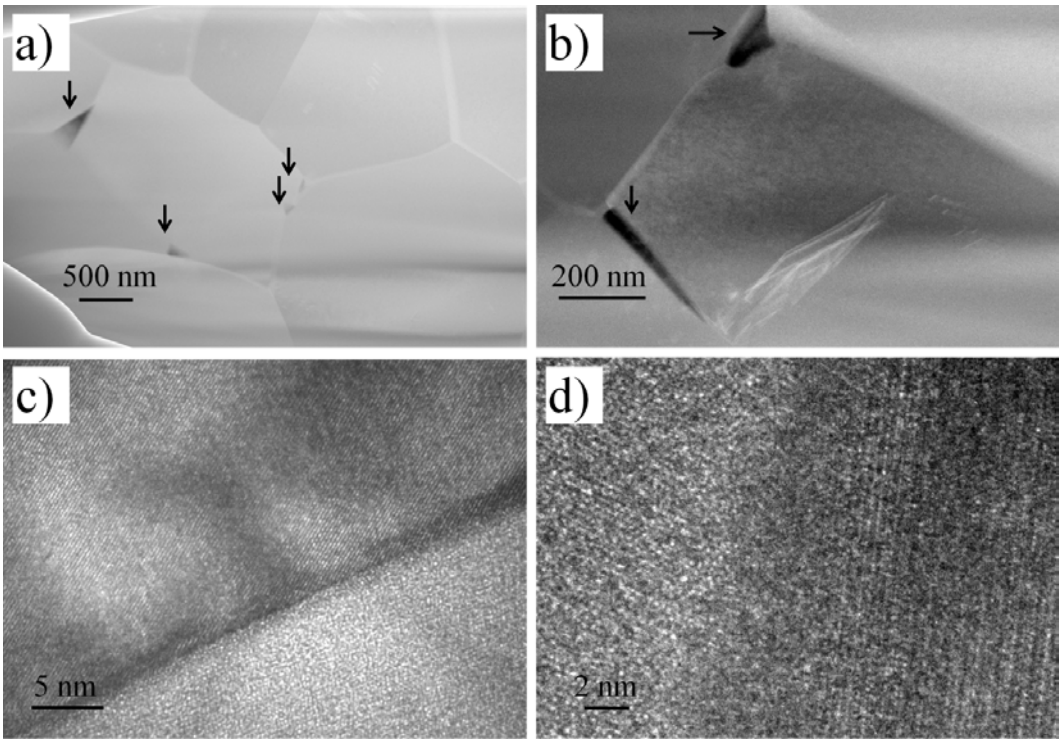

Fig. 4 Transmission electron microscopy images of hipped LLTO ceramics: a) and b) HAADF-STEM images, showing pores along grain boundaries and at triple points, c) and d) high-resolution TEM images of grain boundaries with no secondary phases

In summary, the sintered and hipped LLTO samples have a cubic structure, with a grain size ~2.42 μm, equiaxed grain morphology, near full theoretical density (~99%), strong bonding (i.e., evidence of transgranular fracture) across the grain boundaries, and clean grain boundaries with no second phases. Thus, these LLTO samples should exhibit high grain boundary and total ionic conductivity.

Figure 5 is a representative impedance spectrum at room temperature for the sintered and hipped LLTO. Figure 5 shows the impedance spectrum over the total frequency range investigated. The inset in Fig. 5 is a magnified view of the high frequency region. From Fig. 5 it can be observed that the impedance spectrum of the sintered and hipped LLTO sample contains 2 semi-circles and an inclined spike in the low frequency region. All 6 sintered and hipped LLTO samples exhibited similar spectra. The equivalent circuit, $(R_g)(R_{gb}Q_{gb})(Q_{el})$, shown in Fig. 5, was used to model the impedance spectra where the subscripts g, gb, and el refer to the grains, grain boundaries, and blocking electrode, and R is the resistance and Q is a constant phase element.[8,20–22] The appearance of the inclined spike at low frequencies in the curve is an indication that the sintered and hipped LLTO is an ionic conductor, since we are using Li-ion blocking Pt electrodes.[6–13,15–17] This is in agreement with previous results for sintered LLTO.[3–5,9–13,15–17] The capacitance, C, for the low frequency tail was determined using $C = (2\pi f\ Z'')^{-1}$, where f is the measured

frequency and Z'' is the corresponding imaginary value of the impedance at this frequency.[8] The capacitance values for the low frequency inclined spike are 6.39 ± 0.82 x 10^{-7} F. This capacitance value is characteristic of a double layer capacitance (10^{-7}–10^{-5} F), associated with the sample-blocking electrode interface,[8] thus, confirming that the low frequency spike is related to the Li-ion blocking Pt electrode interface. The capacitance of the low frequency semi-circle calculated using the relation, $C = (2\pi f\, R)^{-1}$, where R is the diameter of the semi-circle and f is the frequency of the semi-circle maximum, and was found to be 1.66 ± 0.52 x 10^{-8} F. This capacitance value is characteristic of grain boundary capacitance (10^{-11}–10^{-8} F).[8] Furthermore, this value is near the high end of values associated with grain boundary capacitance for well-sintered materials.[8] This is in agreement with the high relative density (~99%) obtained using the combined sintering and hipping method. The high frequency spectrum shown in the inset is typically associated with the grain resistance.[6–13,15–17] As shown in the inset, we could not obtain a complete semi-circle at higher frequencies because, we had reached the frequency limit of the instrument (7 MHz).

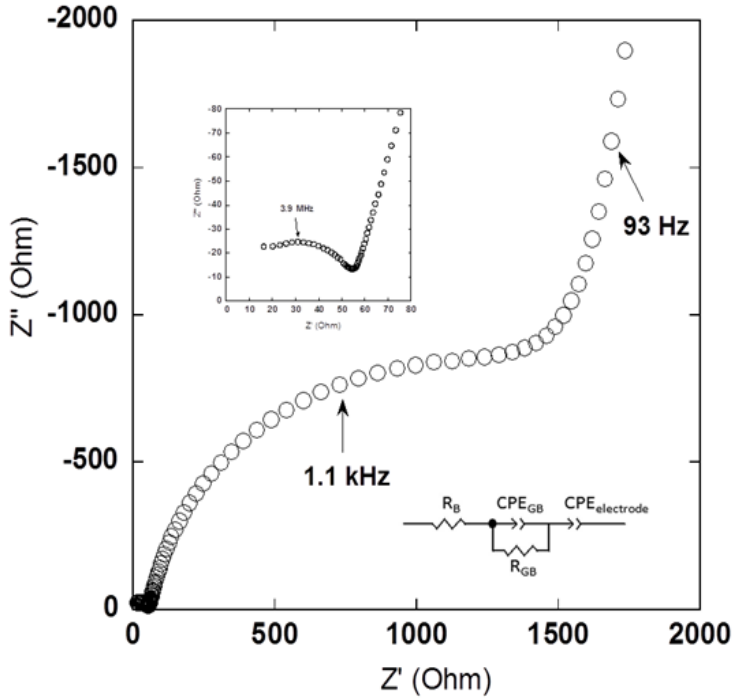

Fig. 5 Room temperature impedance spectrum of $Li_{0.35}La_{0.55}TiO_3$. The inset is a magnified view of the high frequency region.

To further confirm that the low frequency semi-circle was associated with a grain boundary and not a surface film, one sample was repolished and the thickness reduced from 0.0732 cm to 0.0476 cm, after which Pt was sputter-coated onto the top and bottom surfaces of the specimen and the impedance was measured. Since

both the grain and grain boundary resistances are proportional to specimen thickness, the ratio of the resistances should be constant independent of the specimen thickness if the low frequency semi-circle is, indeed, associated with grain boundary resistance. However, if the low frequency semi-circle is associated with a surface film resistance, instead, then the ratio of the grain resistance to the resistance associated with the low frequency semi-circle (surface film) should decrease with specimen thickness. No change was observed in the ratio of grain resistance to the resistance associated with the low-frequency semi-circle between the original and the thinned specimen sample, suggesting that the low frequency semi-circle is, indeed, due to grain boundary resistance. With our interpretation validated, the experimental data was fit using the equivalent circuit model above. Values for R_b and R_{gb} ($R_{gb}=R_{total}-R_g$, where $R_{total,}$ is total resistance) determined using ZView along with the sample dimensions allowed for determination of the lattice and grain boundary conductivities.

The lattice conductivity, σ_g, values were $1.50 \pm 0.21 \times 10^{-3}$ S/cm for the sintered and hipped LLTO. These values are typical for cubic LLTO of similar composition at room temperature.[5,13,15] The grain boundary conductivity, $\sigma_{gb,}$ values were $3.82 \pm 0.11 \times 10^{-5}$ S/cm for the sintered and hipped LLTO at room temperature. The total conductivity, σ_T, values for the sintered and hipped LLTO were $3.73 \pm 0.16 \times 10^{-5}$ S/cm, which are close to values for the grain boundary conductivity.

To determine the electronic conductivity of the sintered and hipped LLTO, DC polarization was undertaken. Figure 6 is a typical example of the DC polarization behavior. It can be seen that there is an exponential decay of the current with time. The electronic conductivity, $\sigma_{e,}$ was estimated from the steady state current.[20,21] The electronic conductivity values at room temperature were $3.62 \pm 0.09 \times 10^{-8}$ S/cm. These values are in agreement with previous values for LLTO (1×10^{-8} [(4)], 5×10^{-9} [(9)] and 5×10^{-9} [(19)] S/cm). The ionic transfer number determined using the electronic and total ionic conductivity was ~1, confirming that LLTO is an ionic conductor, in agreement with the shape of the curve (inclined spike at low frequencies using Li-ion blocking electrodes) in Fig. 5.

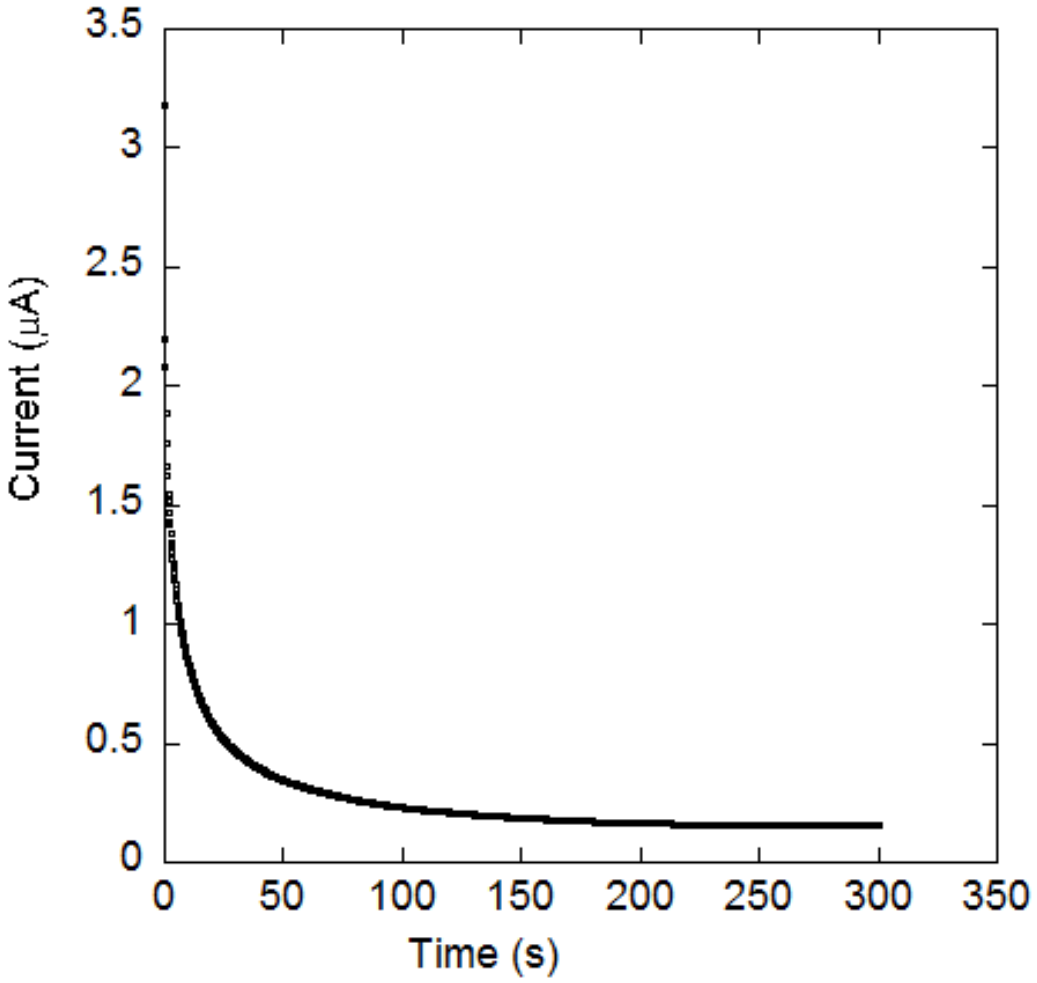

Fig. 6 Representative DC polarization curve of $Li_{0.35}La_{0.55}TiO_3$ at room temperature

The grain boundary and total conductivities at room temperature for the hipped and sintered material can be compared to LLTO samples of similar composition that were only sintered at 1,200 °C. For the case of the LLTO with relative densities between 90–94%, the total conductivities were in the range of 2–3 x 10^{-5} S/cm.[3–5,9,11–13,15] These values are only slightly lower to what was obtained in this study, where the relative density of the LLTO was near full theoretical (~99%). In addition, it should be noted that for LLTO that was consolidated by spark plasma, sintering to a high relative density of 98.5% had a total conductivity of only 5.8 x 10^{-6} S/cm.[22] It was believed that that sintered and hipped LLTO with a relative density (99%) near full theoretical would exhibit total conductivity values approaching values for lattice conductivity, as is the case other solid-state Li-ion conductors—$Li_7La_3Zr_2O_{12}$[23,24] and $Li_{1.3}Ti_{1.7}Al_{0.3}(PO_4)_3$.[25] The results of this study combined with spark plasma sintering results suggest that porosity is not the reason for the low grain boundary conductivity in LLTO. Reasons why the grain boundary conductivity for the sintered and hipped LLTO remain low compared to lattice

conductivity values even when the material is near full theoretical density are not known. However, recently a very detailed electron microscopy characterization using sub-angstrom-resolution STEM imaging combined with electron energy loss spectroscopy (EELS) on over 30 grain boundaries in sintered $Li_{0.33}La_{0.56}TiO_3$ was conducted.[26] In this study, a majority of the grain boundaries did not exhibit the perovskite structure. Instead, these grain boundaries were composed of a 2–3 unit cell thick region where the major component was a binary Ti-O compound depleted of both Li and La. Since, no Li is present, these grain boundaries exhibit poor Li transport. Consequently, if these results are correct, then this could possibly explain the low grain boundary conductivity of the sintered and hipped LLTO materials of near full theoretical density.

4. Conclusions

In summary, sintered and hipped $Li_{0.35}La_{0.55}TiO_3$ samples exhibited a cubic structure, equiaxed grain morphology, (~2.42 μm), near full theoretical density (~99%), strong bonding across the grain boundaries (as evidenced by transgranular fracture), and clean grain boundaries with no secondary phases observed. The lattice conductivity at room temperature was ~1.5 x 10^{-3} S/cm, typical for cubic LLTO of similar composition. The electronic conductivity was ~3.6 x 10^{-8} S/cm, in agreement with literature values. The room temperature grain boundary conductivity values ranged from ~3.8 x 10^{-5} S/cm for sintered and hipped LLTO. These values are slightly higher than those obtained using conventional solid-sate sintering. Even though the sintering followed by hipping method lead to a material with near full theoretical density, this procedure still yielded total conductivity values that were significantly lower than lattice conductivity values. These results, combined with detailed electron microscopy characterization, suggest that in order to increase the grain boundary conductivity of LLTO, the addition of an amorphous Li-ion conducting phase is required; achieving full density alone is not sufficient.

5. References

1. Kowalczk I, Read J, Salomon M. Pure Appl. Chem. 2007;5:851–860.
2. Wolfenstine J. J. Mater. Sci. 2008;43:7247–7249.
3. Kawai H, Kuwano J. J. Electrochem. Soc. 1994;141:L78–L79.
4. Inaguma Y, Chen CQ, Itoh M, Nakamura T, Uchida T, Ikuta H, Wakihara M. Solid State. Commun. 1994;86:689–693.
5. Stramare S, Thangadurai V, Weppner W. Chem. Mater. 2003;15:3974–3990.
6. Huggins RA. Ionics. 2002;8:300–313.
7. Bauerle JE. Phys. Chem. Solids. 1969;30:2657–2670.
8. Irvine JTS, Sinclair DC, West AR. Adv. Mater. 1990;2:132–138.
9. Sutorik AC, Green MD, Cooper C, Wolfenstine J, Gilde G. J. Mater. Sci. 2012;47:6992–7002.
10. Chiang YM, Birnie D, Kingery WD. Physical Ceramics, John Wiley & Sons, Inc., New York, 1997.
11. Kang KY, Fung KZ, Leu IC. J. Alloys Comp. 2007;438:207–210.
12. Ban CW, Choi GM. Solid State Ionics. 2001;140:285–290.
13. Harada Y, Iahigaki T, Kawai H, Kuwano J. Solid State Ionics. 1998;108:407–413.
14. Cooper C, Sutorik AC, Wright J, Luoto III EA, Gilde G, Wolfenstine J. Advanced Engineering Materials. 2014:16:755–759.
15. Harada Y, Hirakoso Y, Kawai H, Kuwano J. Solid State Ionics. 1999;121:245–251.
16. Chen CH, Amine K. Solid State Ionics. 2001;144:51–57.
17. Yang JY, Wang JW, Fung KZ. J. Alloys Comp. 2008;458:415–427.
18. Munro R. J. Am. Ceram. Soc. 1997;80:1919–1928.
19. Bohnke O, Bonke C, Forquet JL. Solid State Ionics. 1996;91:21–31.
20. Kennedy JH, Kimura N, Stuber SM. J. Electrochem. Soc. 1982;129:1968–1973.

21. Allen JL, Thompson T, Sakamoto J, Becker CR, Jow TR, Wolfenstine J. J. Power Sources. 2014;254:204–208.

22. Mei A, Jian QH, Lin YH, Nan CW. J. Alloys Comp. 2009;486:871–875.

23. Rangasamy E, Wolfenstine J, Sakamoto J. Solid State Ionics. 2012;206:28–32.

24. Allen JL, Wolfenstine J, Rangasamy E, Sakamoto J. J. Power Sources. 2012;206:315–319.

25. Aono H, Sugimoto E, Sadaoka Y, Imanaka N, Adachi G. J. Electrochem. Soc. 1990;137:1023–1027.

26. Ma C, Chen K, Liang C, Nan CW, Ishikawa R, More K, Chi M. Energy & Environmental Science. 2014;7:1638–1642.

1 (PDF) DEFENSE TECHNICAL INFORMATION CTR DTIC OCA

2 (PDF) DIRECTOR US ARMY RESEARCH LAB RDRL CIO LL IMAL HRA MAIL & RECORDS MGMT

1 (PDF) GOVT PRINTG OFC A MALHOTRA

7 (PDF) DIR USARL RDRL SED C
J ALLEN
C LUNDGREN
J READ
J WOLFENSTINE
RDRL WMM E
J ADAMS
V BLAIR
J P SINGH

INTENTIONALLY LEFT BLANK.